Nuclear Engineering and Technology 54 (2022) 2592–2598

Contents lists available at ScienceDirect

Nuclear Engineering and Technology

journal homepage: www.elsevier.com/locate/net

Original Article

Optimized TOF-PET detector using scintillation crystal array for brain imaging

Hyuntae Leem, Yong Choi*, Jiwoong Jung**, Kuntai Park, Yeonkyeong Kim, Jin Ho Jung

Molecular Imaging Research & Education (MiRe) Laboratory, Department of Electronic Engineering, Sogang University, 35 Baekbeom-ro, Mapo-gu, Seoul, 04107, South Korea

ARTICLE INFO

Article history:
Received 26 July 2021
Received in revised form
19 January 2022
Accepted 9 February 2022
Available online 10 February 2022

Keywords:
Time-of-flight
PET
Scintillation crystal
CRT
LYSO
Specular reflector
Diffusive reflector

ABSTRACT

Research groups in the field of PET instrumentation are studying time-of-flight(TOF) technology to improve the signal-to-noise ratio of PET images. Scintillation light transport and collection plays an important role in improving the coincidence resolving time(CRT) of PET detector based on a pixelated crystal array.

Four crystal arrays were designed by the different optical reflection configuration such as external reflectors and surface treatment on the CRT and compared with the light output, energy resolution and CRT. The design proposed in the study was composed of 8 × 8 LYSO crystal array consisted of 3 × 3 × 15 mm^3 pixels. The entrance side was roughened while the other five surfaces were polished. Four sides of all crystal pixels were wrapped with ESR-film, and the entrance surface was covered by Teflon-tape. The design provided an excellent timing resolution of 210 ps and improved the CRT by 16% compared to the conventional method using a polishing treatment and ESR-film.

This study provided a method for improving the light output and CRT of a pixelated scintillation crystal-based brain TOF PET detector. The proposed configuration might be an attractive detector design for TOF brain PET requiring fast timing performance with high cost-effectiveness.

1. Introduction

Positron-emission tomography (PET) is a nuclear medicine imaging system that can provide functional images to diagnose and monitor human diseases. Recently, there has been great interest in the development of dedicated brain PET for the diagnosis of neurological disorders such as dementia and movement impairments because a dedicated brain PET could offer superior human-brain imaging, achieving high sensitivity, spatial resolution, and image quality as compared with the conventional whole-body PET [1–4]. Many research groups have being developed the dedicated brain PET based on cylindrical detector arrangement [1,5]. The various PET geometries were also designed including helmet shape, partial sphere, and dodecahedral shape to make a high-sensitivity brain PET systems [6–8].

Time-of-flight (TOF) technology reduces the propagation of noise along the lines of response (LOR) by measuring the detected time difference of the two 511 keV gamma rays. Noise reduction can be equated to an increase in the SNR, NEC, and sensitivity, allowing the reduction in radiation dose and/or scanning time [9–11]. TOF SNR gain can be described by $\sqrt{D/(c \times \Delta t)}$ where D is the object size, c is the speed of light, and Δt is the timing resolution. Therefore, faster timing resolution is required when the object size is smaller. For example, when the size of the imaging object is 200 mm, as is the human brain, the TOF PET with CRT of 200 ps could ideally increase SNR gain by 20% compared to TOF PET systems with CRT of 400 ps. Most of the commercial PET systems have insufficient TOF performance (about 210–400 ps) for brain imaging because there is a marginal gain in the SNR and NEC for small imaging objects [9,12–15]. Therefore, the TOF-PET detector for a dedicated brain PET having a smaller field of view (FOV) of 200 mm requires CRT of below 200 ps to achieve a meaningful gain in SNR.

The CRT of scintillation crystal based PET detector is determined by factors such as the intrinsic properties of the scintillation crystal (light yield, and the intrinsic rise and decay times of scintillation light) and the characteristics of the photodetector (photon detection efficiency, noise, and dark count rate) [16]. Additionally, the important factors in CRT are scintillation light transport and the

* Corresponding author.
** Corresponding author.
E-mail address: ychoi@sogang.ac.kr (Y. Choi).

https://doi.org/10.1016/j.net.2022.02.009

scintillation light collection, which can be improved by optimizing the optical properties and the surface conditions of the scintillation crystals.

In recent studies, the effect of various surface-roughened configurations in scintillation crystals was demonstrated by Monte Carlo simulation and experiments conducted to improve both light transport and light collection. The scintillation crystal design providing the considerable improvement in CRT was to have one side partly (75%) roughened and other sides polished [17]. The effect of light sharing in the scintillation crystal array was also studied by comparing the ESR film and the air gap between the scintillation crystals. The scintillation crystal array using an air gap between crystals was reported to collect 16% more light than the scintillation crystal array using ESR film between the scintillation crystals [18]. These studies demonstrated that the surface-roughened configuration and the light-sharing method could improve the transport and collection of scintillation light by reducing the travel time of photons and scintillation light loss by decreasing multiple reflections within the crystal. However, the results in the reported studies used a single scintillation crystal or a PET detector block consisting of a few large scintillation crystals. To determine the optimal scintillation crystal array design for brain PET by optimizing the optical reflection configurations, a comparative evaluation at the level of the detector-block could be applied to dedicated brain PET.

In this study, four different crystal arrays with different surface treatments and reflective materials were fabricated to evaluate the CRT and light-output performance. All designs consisted of 8 × 8 pixelated scintillation crystals to investigate the effect of optical properties and the surface conditions at the level of the detector-block. The results of this study will be employed to develop a dedicated brain PET system having about 200 ps of timing resolution and about 2.0 mm of spatial resolution at center of FOV.

2. Materials and methods

2.1. Optical scintillation crystal array designs

Four different crystal arrays with different optical conditions such as surface treatment and reflective materials were fabricated (Crystal Photonics, Inc., Sanford, Florida) as illustrated in Fig. 1. The active area of MPPC (3.0 × 3.0 mm^2) was slightly smaller than the cross section of a crystal (3.11 × 3.11 mm^2 or 3.19 × 3.19 mm^2) to increase the sensitivity of the detector while minimizing the dead-space by gaps among the crystal pixels. The crystal having a larger cross-section than that of SiPM could achieve high photon detection efficiency while might degrade energy resolution and light collection [19].

Design (1) was composed of an 8 × 8 array of LYSO:Ce pixels which were mechanically polished by a diamond burr (500 grit) [17]. The pixel size was 3.11 × 3.11 × 15 mm^3. All LYSO crystal pixels were isolated by ESR film (specular reflector) and the outside of the array was wrapped with ESR film.

Design (2) was composed of 8 × 8 LYSO:Ce pixels of 3.11 × 3.11 × 15 mm^3. One of the four side surfaces was roughened on 75% of its surface, and the other three sides were polished, as shown in Fig. 1 and called “partly roughened one side” in this study. All crystal pixels were isolated by ESR film, and the outside of the array was wrapped by ESR film.

Design (3) was composed of 8 × 8 LYSO:Ce pixels of 3.11 × 3.11 × 15 mm^3. The entrance side (the direction of gamma-ray incidence) was roughened while the other five surfaces were polished and called “roughened entrance surface” in this study. Four sides of all crystal pixels were wrapped by ESR film, and the entrance surface was covered by Teflon tape (diffusive reflector). This reflector configuration was called the “hybrid reflector” in this study.

Design (4) was composed of an 8 × 8 LYSO (3.19 × 3.19 × 15 mm^3) using the partly roughened one side (One of the four side surfaces was roughened on 75%) and the air gap between the crystal pixels. ESR film was wrapped on the outside of the array.

2.2. Experimental setup and data acquisition

Fig. 2 shows the experimental setup for CRT and light output measurement. The distance between the two detector modules was 40 mm, and Na-22 was located in front of the reference detector to increase the probability of detecting coincident events. Each detector consisted of an 8 × 8 array MPPC (S13361-3050AE-08, Hamamatsu, Japan) with a pixel size of 3.00 × 3.00 mm^2 and a LYSO crystal array with different designs. The reference detector was fabricated with a 3 × 3 × 15 mm^3 LSO:Ce scintillation crystal, with all surfaces polished, wrapped with Teflon tape, and coupled to the center pixel of the MPPC array.

Application specific integrated circuit (ASIC) evaluation board (TOFPET2 ASIC, PETSYS, Portugal) were utilized to acquire and measure the output signals of all MPPC channels. The ASIC consisted of the pre-amplifiers, the channel trigger-circuit, the time-to-digital converters (TDC) and charge-to-digital converters (QDC) on 64 channels [20,21]. The TDC was used to measure the arrival times of scintillation photons and had a resolution of 30 ps with running with a clock cycle of 200 MHz. The QDC could integrate the charges up to 1500 pC to measure the energy values. The ASIC also provided signal-gain adjustment and amplification, pulse discrimination, and amplitude measurement. A low threshold voltage of 5 mV was set to measure the arrival time of the scintillation photons on the single-photon level. Baselines on all channels was adjusted during calibration process to be ensured that the threshold of trigger-circuit about all channels was equally adjusted [20]. The bias voltage of the MPPC was set on 56.0 V (over-voltage: 3.0 V) at 23 °C [22]. The mini-thermostat was used to maintain the temperature of the photo-sensor. The experiments were repeated five times to examine the reproducibility of the crystal array performance.

The intensity-center-of-gravity algorithm was used to calculate the position of the events in Designs (4). The formula for an $m \times n$ MPPC array is given by

$$X = \frac{\sum_{i=1}^{m}\sum_{j}^{n} w(i,j) \times P_{i,j} \times j}{\sum_{i=1}^{m}\sum_{j=1}^{n} w(i,j) \times P_{i,j}} \quad (1)$$

$$Y = \frac{\sum_{i=1}^{m}\sum_{j}^{n} w(i,j) \times P_{i,j} \times i}{\sum_{i=1}^{m}\sum_{j=1}^{n} w(i,j) \times P_{i,j}} \quad (2)$$

$$w(i,j) = P_{i,j} \quad (3)$$

where X and Y were the calculated coordinates of a scintillation event, and $w(i, j)$ is the weighting factor equivalent to the intensity of the detected scintillation light output of pixel = $P_{i,j}$. The intensity-center-of-gravity algorithm applied a weight factor equivalent to the signal values themselves [23,24].

The $CRT_{det\text{-}det}$ was calculated using the CRT of reference scintillator ($CRT_{ref\text{-}ref}$), and that between detector module and reference detector ($CRT_{det\text{-}ref}$) pair using the formula as given in [24–26].

$$CRT_{det-det} = \sqrt{2} \times \sqrt{CRT_{det-ref}^2 - \left(\frac{CRT_{ref-ref}}{\sqrt{2}}\right)^2} \quad (4)$$

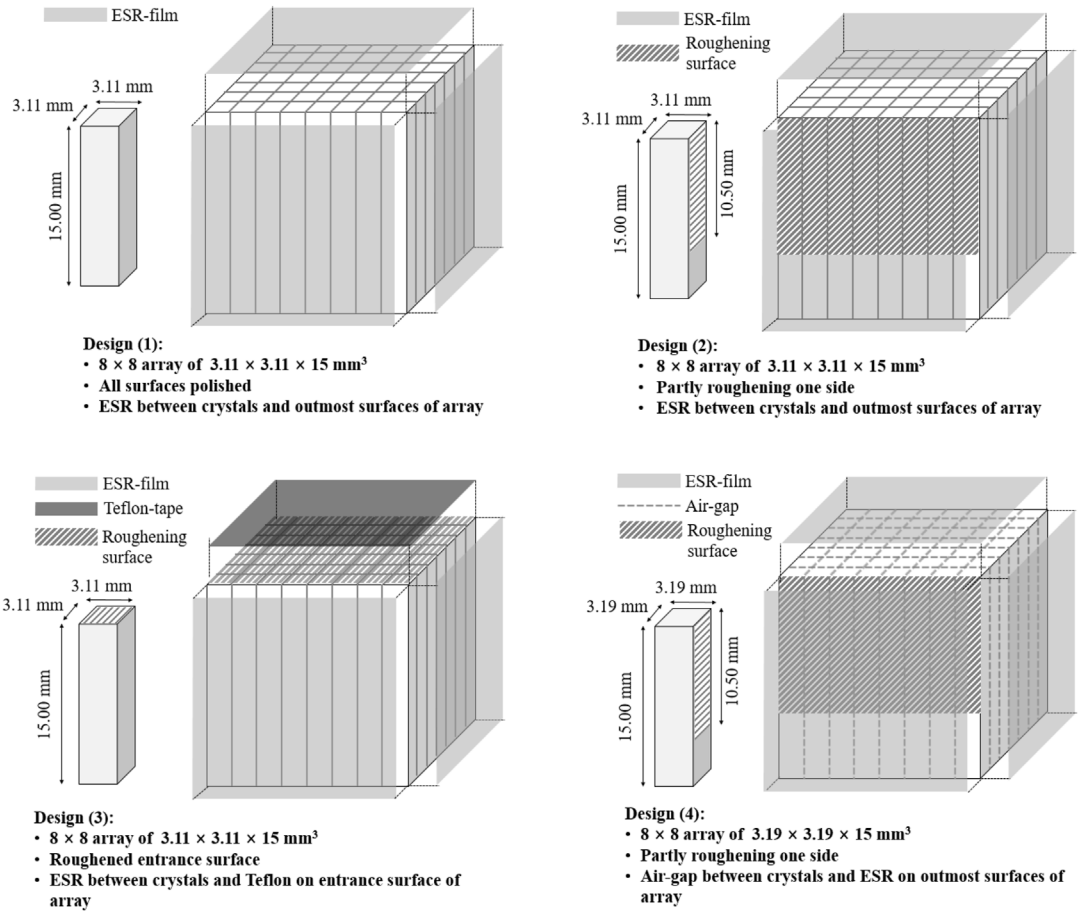

Fig. 1. Crystal array schemes with different surface treatments and reflective materials. The roughened surfaces are indicated by hatched lines. The bottom surface of the crystal was coupled to the photosensor.

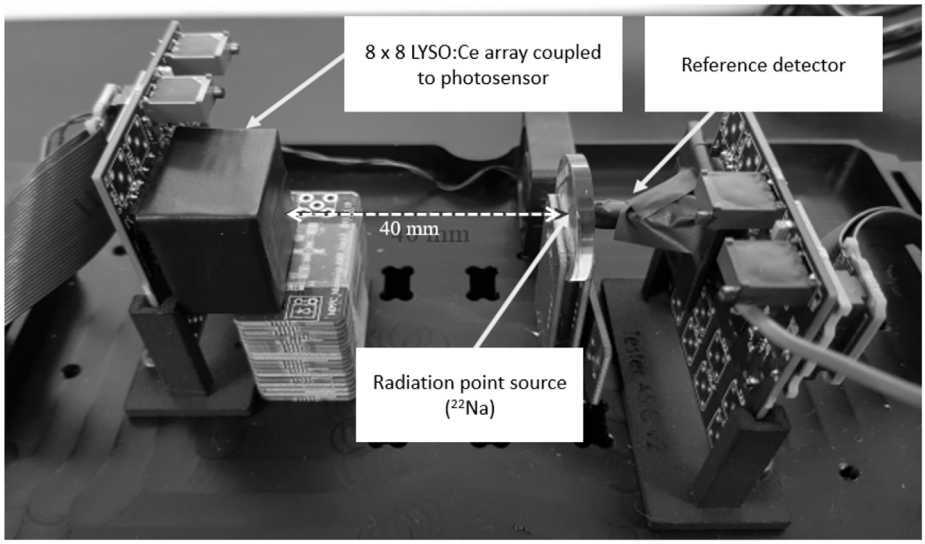

Fig. 2. Experimental setup for CRT measurement. The array detector (MPPC coupled to LYSO array) was located on the left side and the reference detector (MPPC coupled to a single LSO crystal) was located on the right side.

Table 1
CRT of all crystal pixels and center pixel.

Design	CRT(average of all pixels)		CRT (center pixel)	
Design (1)	282 ± 5 ps	(1.00)	251 ± 6 ps	(1.00)
Design (2)	259 ± 2 ps	(0.92)	221 ± 5 ps	(0.88)
Design (3)	237 ± 2 ps	(0.84)	210 ± 6 ps	(0.83)
Design (4)	362 ± 8 ps	(1.28)	287 ± 11 ps	(1.14)

3. Results

3.1. Coincidence resolving time

Table 1 presents the average CRT and the CRT of the center pixel in all scintillation crystal designs. The results in each design were normalized to Design (1), which is typically used in conventional PET detector blocks. Table 1 clearly shows the difference in CRT obtained using the different optical conditions such as surface treatment and reflector materials. Design (1) showed CRT of about 282 ± 5 ps FWHM. Design (2) and (3) showed improvements of 8% and 16%, respectively, in the CRT compared to Design (1). Design (3) showed the best average CRT (237 ± 2 ps FWHM) for all pixels and the best CRT (210 ± 6 ps FWHM) for the center pixel. The CRT measured using Design (2) showed 10% deterioration compared to that of Design (3).

We evaluated the effect of different reflecting materials (ESR film vs air gap) on the CRT by comparing Designs (2) and (4) consisting of crystal pixels using partly roughened on one side. The color maps in Fig. 3 show the CRT difference measured using the two scintillation crystal arrays (Designs (2) and (4)). The average CRT of Design (2) using ESR film was superior by 28% (=103 ps FWHM) to that of Design (4) using an air gap.

3.2. Light output

The light output of different scintillation crystal array designs was evaluated by measuring the photo-peak position at 511 keV. The light output of all crystal array designs was averaged and the result is presented in Table 2. The highest light output was achieved by Design (3), which increased the light output by 32% compared to Design (1). The optical reflection configurations of Design (2) also provided an 18% higher light output than Design (1) because of the favorite surface treatment. However, Design (2) provided 14% less light output than Design (3).

We evaluated the effect of air-gap on light output by comparing Designs (2) and (4) with the same surface treatment condition. The light output of Design (4) using the air-gap was considerably lower than that of Design (2). Fig. 4 shows the photo-peak (at 511 keV) position map of all crystal arrays. We observed an average light loss of 39% in Design (4) compared to Design (2). The light output of the outside pixels of Design (4) was decreased by over 34% than that of the center pixel.

3.3. Energy resolution

The energy resolutions of all crystal pixels are summarized in Table 3. Designs (1), (2), and (3) provided similar energy resolution performance, from 7% to 10%, whereas Designs (4) provided low energy resolution, from 12 to 13%. Fig. 5 shows the energy resolution map for all pixels of Designs (2) and (4) with the same surface treatment condition. The crystal array using the air gap provided a lower energy resolution than the one using ESR film, and the energy resolution deteriorated in the outside crystal pixels compared to the center crystal pixels because of increased light loss.

4. Discussion

In this study, the effect of the optical reflection configurations of pixelated scintillation crystals on the CRT was assessed by comparing various LYSO crystal arrays for a dedicated brain PET. The partly roughened surface of Designs (2) and (3) improved the CRT compared to Design (1) with all polished surfaces because it could minimize the light transit time in the scintillation crystal. The results of this study showed a similar trend to those previous study which reported that the partly roughened surface provided better CRT than the polished surfaces [16].

Design (3) showed a better CRT (14%) than Design (2) due to the structural advantages of the hybrid reflector. The Teflon-tape covering on the entrance surface could minimize loose adhesion caused by the gap in the crystal edge [27]. This reflector combination was able to improve the CRT by increasing the light output due to these structural advantages as shown in Fig. 6.

The hybrid reflector in Design (3) was designed by focusing on improvement of the reflectance probability on the entrance surface. Reflectance probability was different as function of incidence

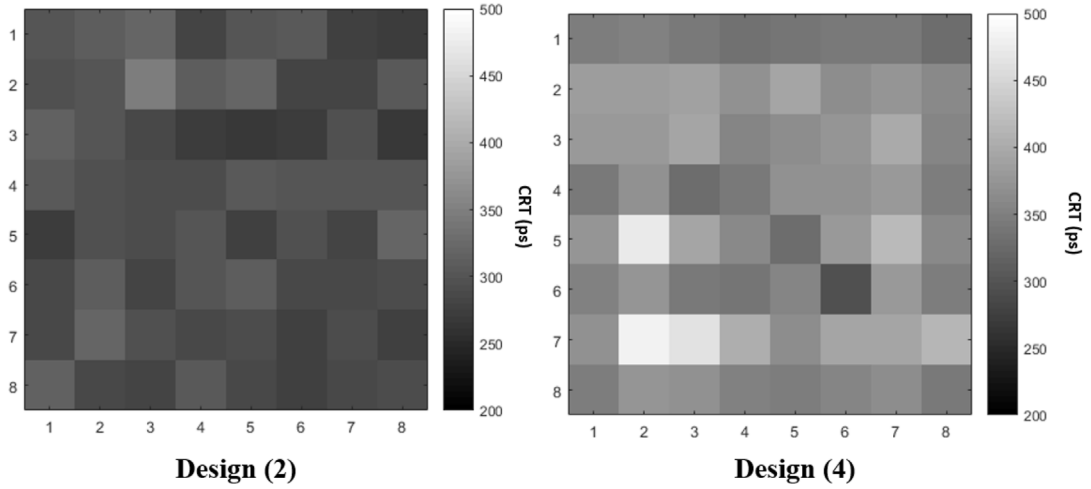

Fig. 3. Color maps showed the CRT of all scintillation crystal pixels of Designs (2) and (4). The average CRT of Design (2) using ESR film was superior to that of Design (4) using an air gap by 103 ps FWHM.

Table 2
Average light output of all pixels and light output of the center pixel.

Designs	Light output (Average of all pixels)		Light output (Center pixel)	
Design (1)	264 ± 2	(1.00)	279 ± 4	(1.00)
Design (2)	312 ± 2	(1.18)	320 ± 3	(1.15)
Design (3)	349 ± 1	(1.32)	357 ± 3	(1.28)
Design (4)	193 ± 3	(0.73)	214 ± 6	(0.77)

angles for roughed or polished surface. Teflon showed higher reflectivity and lower transmittance than ESR (using grease) for rough surface and the rough surface coupled with Teflon showed large difference of reflectivity as compared with the chemically etched and the mechanically polished [27,28]. In addition, the entrance-surface roughing was the best selection satisfying the timing performance as well as the cost-effectiveness and productivity [17]. The roughened entrance surface covered with Teflon-tape having diffusive reflectivity provided the better light output in this study than partly roughened one side surfaces covered with ESR film with specular reflectivity because Teflon-tape on the roughened entrance surface reduced the number of photons trapped in the crystal, increasing the reflectance probability toward the MPPCs. The diffusive reflector on the roughened surface increased the reflection probability of low incidence angles compared to the ESR-film on the roughened surface, as reported in previous studies [17,28,29]. Therefore, the hybrid reflector in Design (3) was able to provide the best light collection efficiency among the various crystal array designs due to these structural and optical advantages.

Table 3
Average energy resolutions of all crystal pixels and that of the center pixel.

Design	Average energy resolution (%) of all crystal pixels	Energy resolution (%) of the center pixel
Design (1)	9	8
Design (2)	9	10
Design (3)	8	7
Design (4)	13	12

Design (4) using the air-gap provided lower light output than Designs (1), (2), and (3). The scintillation light splitting to adjacent MPPCs could reach the dead-space which was the gap of 0.2 mm between the MPPCs causing scintillation light loss. In addition, the light output might decrease because the light transmission path length was increased by expanding the size of the scintillation crystal array block with air-gaps between the scintillation crystals. However, the crystal arrays using reflectors collected more scintillation light by reducing the possibility of reaching the dead space and by decreasing the transmission path length, although a little scintillation light could be reduced by trapping in a crystal [29,30]. The light loss also caused the deterioration of the energy resolution measured in Design (4), as shown in Table 3 and Fig. 6. The CRT

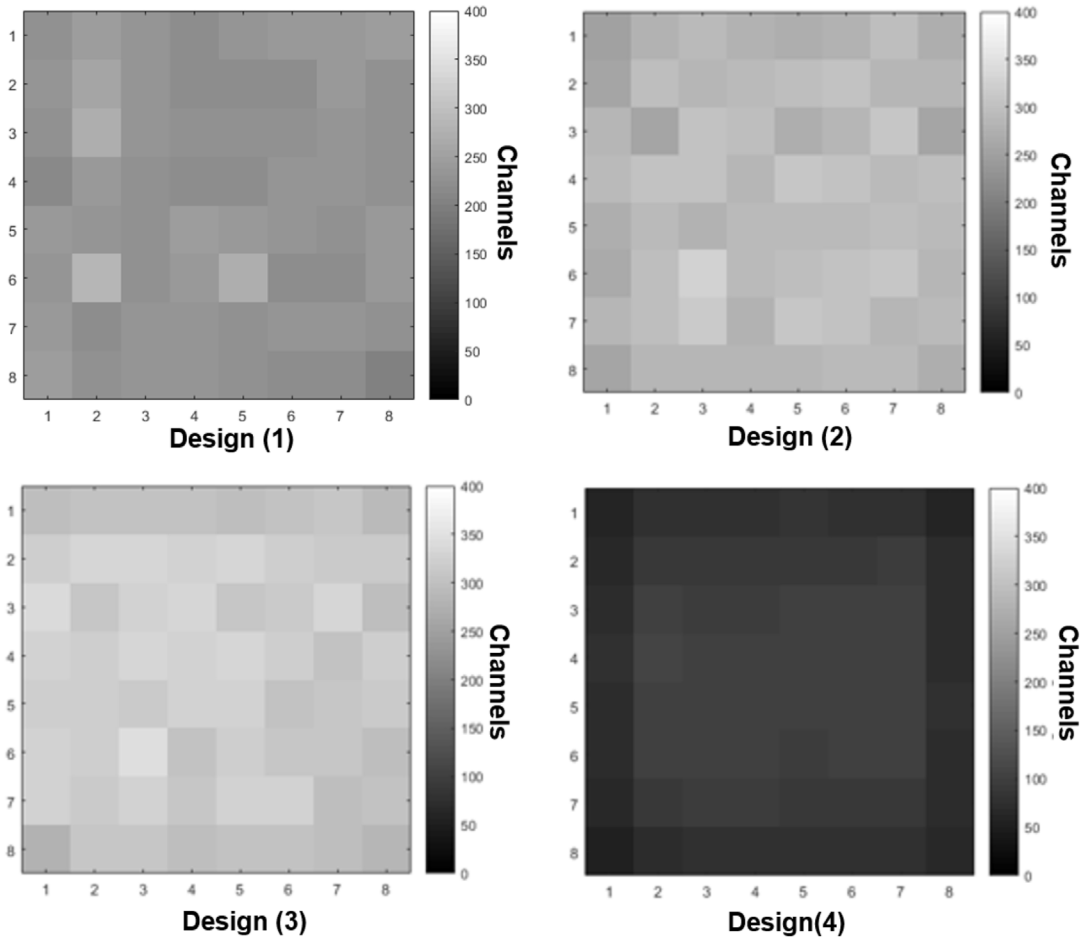

Fig. 4. Photo-peak position map of all crystal pixels in Designs (1) to (4).

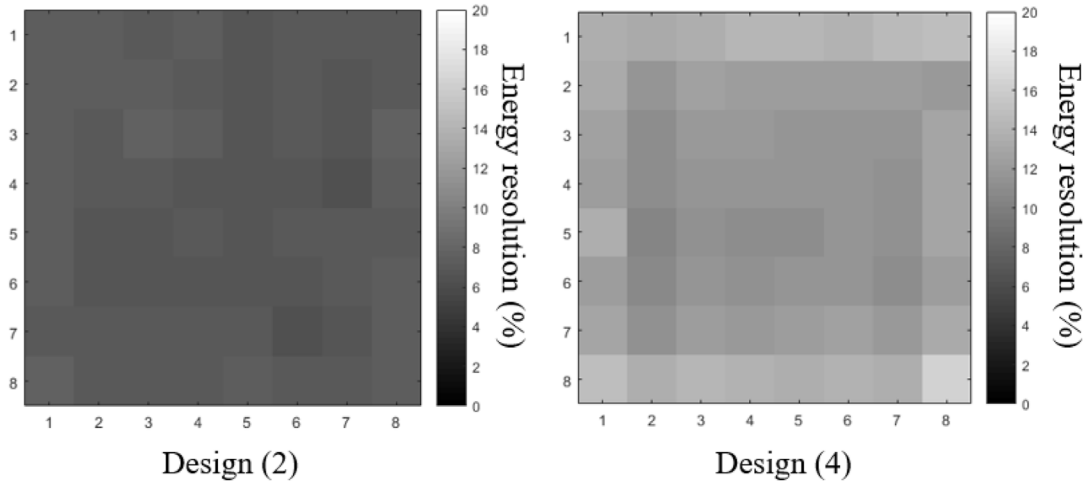

Fig. 5. Energy resolution map of 64 crystal pixels in Designs (2) and (4). Designs (1) and (2) are not presented in this figure, because the energy resolution of Design (2) was similar to that of Designs (1) and (3).

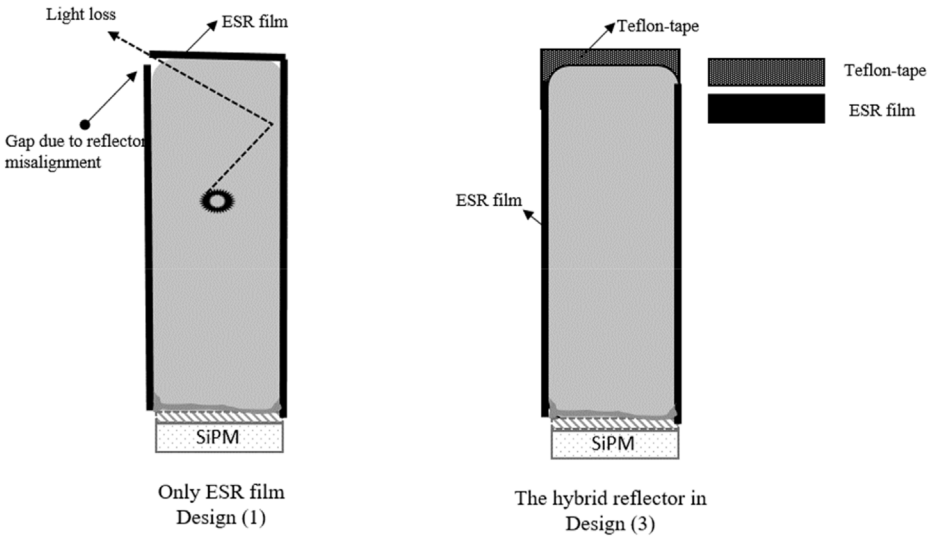

Fig. 6. Different cases for reflector application to the crystal. The hybrid reflector in Design (3) minimized the light loss due to the gap between the edge of the ESR-film.

measured using Design (4) was considerably deteriorated because of the low light output. The scintillation photons could be absorbed or lost by passing through many crystal pixels and air-gaps. These results showed different trends than those of the previous study because the PET detector in the reported study utilized a detector block consisting of a few crystal pixels and an SiPM with a large active area [18].

5. Conclusion

The results of this study focusing on the optical reflection configurations of pixelated crystal arrays provided a method for improving the light output and CRT of scintillation crystal-based brain TOF PET detectors. The crystal array design using a roughened entrance surface with a hybrid reflector was proposed and demonstrated an excellent timing resolution of 210 ps FWHM, which improved the SNR of brain PET images by 2.5 times compared to non-TOF PET images. In addition, the proposed method could decrease the production cost with a good CRT because the manufacturing process of roughening the entrance surface is relatively simple compared to partly roughening one side. Therefore, we concluded that the optical configuration of Design (3) might be an attractive detector design for TOF brain PET system requiring fast timing performance.

Declaration of competing interest

The authors declare that they have no known competing financial interests or personal relationships that could have appeared to influence the work reported in this paper.

Acknowledgment

This research was supported by Basic Science Research Program through the National Research Foundation of Korea (NRF) funded by the Ministry of Education (No. 2019R1I1A1A01041347) and by the Technology development Program (No. S2840619) funded by the Ministry of SMEs and Startups(MSS, Korea) and by the Korea Medical Device Development Fund grant funded by the Korea government (the Ministry of Science and ICT, the Ministry of Trade,

Industry and Energy, the Ministry of Health & Welfare, the Ministry of Food and Drug Safety) (Project Number: KMDF_PR_20200901_0006).

References

[1] J.H. Jung, Y. Choi, J. Jung, S. Kim, H.K. Lim, K.C. Im, C.H. Oh, H. Park, K.M. Kim, J.G. Kim, Development of PET/MRI with insertable PET for simultaneous PET and MR imaging of human brain, Med. Phys. 42 (2015) 2354–2363.

[2] K.J. Hong, Y. Choi, J.H. Jung, J. Kang, W. Hu, H.K. Lim, Y. Huh, S. Kim, J.W. Jung, K.B. Kim, M.S. Song, H.-W. Park, A prototype MR insertable brain PET using tileable GAPD arrays, Med. Phys. 40 (2013) 1–12.

[3] N.Y. Lee, Y. Choi, Simulation studies on depth of interaction effect correction using a Monte Carlo computed system matrix for brain positron emission tomography, Comput. Methods Progr. Biomed. 108 (2012), https://doi.org/10.1016/j.cmpb.2012.05.007.

[4] H. Shin, Y. Choi, Y. Huh, J.H. Jung, T.S. Suh, Conceptual study of brain dedicated PET improving sensitivity, Kor. Soc. Med. Phys. 27 (2016) 236–240.

[5] K. Wienhard, M. Schmand, M.E. Casey, K. Baker, J. Bao, L. Eriksson, W.F. Jones, C. Knoess, M. Lenox, M. Lercher, P. Luk, C. Michel, J.H. Reed, N. Richerzhagen, J. Treffert, S. Vollmar, J.W. Young, W.D. Heiss, R. Nutt, The ECAT HRRT: performance and first clinical application of the new high resolution research tomograph, IEEE Trans. Nucl. Sci. 49 (2002) 104–110.

[6] C. Catana, Development of dedicated brain PET imaging devices: recent advances and future perspectives, J. Nucl. Med. 60 (2019) 1044–1052.

[7] S. Majewski, J. Proffitt, J. Brefczynski-Lewis, A. Stolin, A.G. Weisenberger, W. Xi, R. Wojcik, HelmetPET: A Silicon Photomultiplier Based Wearable Brain Imager, in: IEEE Nucl. Sci. Symp. Conf. Rec, IEEE NSS/MIC/RTSD, Valencia, Spain, Oct. 2011, pp. 23–29.

[8] C.R. Schmidtlein, J.N. Turner, M.O. Thompson, K.C. Mandal, I. Häggström, J. Zhang, J.L. Humm, D.H. Feiglin, A. Krole, Initial performance studies of a wearable brain positron emission tomography camera based on autonomous thin-film digital Geiger avalanche photodiode arrays, J. Med. Imag. 4 (2017), https://doi.org/10.1117/1.JMI.4.1.011003.

[9] J.S. Karp, S. Surti, M.t E.D. Witherspoon, G. Muehllehner, Benefit of time-of-flight in PET: experimental and clinical results, J. Nucl. Med. 48 (2008) 462–470.

[10] H. Thoen, V. Keereman, P. Mollet, R. Van Holen, S. Vandenberghe, Influence of detector pixel size, TOF resolution and DOI on image quality in MR-compatible whole-body PET, Phys. Med. Biol. 58 (2013) 6459–6479.

[11] S. Vandenberghe, E. Mikhaylova, E. D'Hoe, P. Mollet, J.S. Karp, Recent developments in time-of-flight PET, Eur. J. Nucl. Med. Mol. Imag. Phys. 3 (2016). https://ejnmmiphys.springeropen.com/articles/10.1186/s40658-016-0138-3.

[12] M. Conti, Focus on time-of-flight PET: the benefits of improved time resolution, Eur. J. Nucl. Med. Mol. Imag. Phys. 38 (2011) 1147–1157.

[13] E. Yoshida, H. Tashima, G. Akamatsu, Y. Iwao, M. Takahashi, T. Yamashita, T. Yamaya, 245 ps-TOF brain-dedicated PET prototype with a hemispherical detector arrangement, Phys. Med. Biol. 65 (2020). https://iopscience.iop.org/article/10.1088/1361-6560/ab8c91.

[14] S.W. Lee, Y. Cho, J. Kang, J.H. Jung, Development of a multiplexed readout with high position resolution for positron emission tomography, Nucl. Instrum. Methods Phys. Res. A 850 (2017) 42–47.

[15] M. Conti, B. Bendriem, The new opportunities for high time resolution clinical TOF PET, Clin. Transl. Imaging 7 (2019), https://doi.org/10.1007/s40336-019-00316-5.

[16] S. Gundacker, F. Acerbi, E. Auffray, A. Ferri, A. Gola, M.V. Nemallapudi, G. Paternoster, C. Piemonte, P. Lecoq, State of the art timing in TOF-PET detectors with LuAG, GAGG and L(Y)SO scintillators of various sizes coupled to FBK-SiPMs, J. Instrum. 11 (2016). https://iopscience.iop.org/article/10.1088/1748-0221/11/08/P08008.

[17] E. Berg, E. Roncali, S.R. Cherry, Optimizing light transport in scintillation crystals for time-of-flight PET: an experimental and optical Monte Carlo simulation study, Biomed. Opt Express 6 (2015) 2220–2230.

[18] C. Kim, M. Ito, D.L. McDaniel, Effect of Scintillation Crystal Surface Finish in the Light Sharing TOF PET Detector, 2016. IEEE Nucl. Sci. Symp. Conf. Rec, IEEE NSS/MIC/RTSD, Strausbourg, France, 29 Oct.-6 Nov.

[19] C.M. Lavelle, W. Shanks, C. Chiang, M. Nichols, J. Osborne Jr., A. Herschelman, B. Brown, M. Cho, Approaches for single channel large area silicon photomultiplier array readout, AIP Adv. 9 (2019), https://doi.org/10.1063/1.5088503.

[20] V. Nadig, D. Schug, B. Weissler, V. Schulz, Evaluation of the PETsys TOFPET2 ASIC in multi-channel coincidence experiments, Eur. J. Nucl. Med. Mol. Imag. Phys. 30 (2021). https://ejnmmiphys.springeropen.com/articles/10.1186/s40658-021-00370-x.

[21] K.B. Kim, Y. Choi, J.W. Jung, S.W. Lee, H.-J. Choe, H.T. Leem, Analog and digital signal processing method using multi-time-over-threshold and FPGA for PET, Med. Phys. 45 (2018) 4104–4111.

[22] T. Nagano, N. Hosokawa, A. Ishida, R. Tsuchiya, K. Sato, K. Yamamoto, Timing Resolution Dependence on MPPC Geometry and Performance, 2013. IEEE Nucl. Sci. Symp. Med. Imag. Conf., Seoul, Korea (South), 27 Oct.-2 Nov.

[23] C.-Y. Liu, A.L. Goertzen, Improved event positioning in a gamma ray detector using an iterative position-weighted centre-of-gravity algorithm, Phys. Med. Biol. 58 (2013) N189–N200.

[24] H.T. Leem, Y. Choi, K.B. Kim, S. Lee, S. Yamamoto, J.-Y. Yeom, Performance evaluation of a sub-millimeter spatial resolution PET detector module using a digital silicon photomultiplier coupled LGSO array, Nucl. Instrum. Methods Phys. Res. A 846 (2017) 18–22.

[25] H.-J. Choe, Y. Choi, W. Hu, J. Yan, J.H. Jung, Development of capacitive multiplexing circuit for SiPM-based time-of-flight (TOF) PET detector, Phys. Med. Biol. 62 (2017) N120–N133.

[26] M. Aykac, F. Bauer, C.W. Williams, M. Loope, M. Schmand, Timing performance of Hi-Rez detector for time-of-flight (TOF) PET, IEEE Trans. Nucl. Sci. 53 (2006) 1084–1089.

[27] E. Roncali, M.A.M. Shirazi, A. Badano, Modelling the transport of optical photons in scintillation detectors for diagnostic and radiotherapy imaging, Phys. Med. Biol. 62 (2017) R207–R235.

[28] E. Roncali, M. Stockhoff, S.R. Cherry, An integrated model of scintillator-reflector properties for advanced simulations of optical transport, Phys. Med. Biol. 62 (2017) 4811–4830.

[29] D.J.V. Elburg, S.D. Noble, S. Hagey, A. Goertzen, Comparison of acrylic polymer adhesive tapes and silicone optical grease in light sharing detectors for positron emission tomography, Phys. Med. Biol. 63 (2018). https://iopscience.iop.org/article/10.1088/1361-6560/aaa815.

[30] E. Lorincz, G. Erdei, I. Péczeli, C. Steinbach, F. Ujhelyi, T. Bükki, Modeling and optimization of scintillator arrays for PET detectors, IEEE Trans. Nucl. Sci. 57 (2010) 48–54.